



Fan Blade Fatigue Fractures in CFM56-7B Engines

M. R. Fox · W. R. Rossey Jr. · M. Raguet

Submitted: 24 May 2023 / in revised form: 23 June 2023 / Accepted: 26 June 2023 / Published online: 12 July 2023
© ASM International 2023

Abstract The National Transportation Safety Board investigated two accidents involving fan blade fatigue fractures in CFM International CFM56-7B engines. Fatigue cracks developed in the Ti-6Al-4V blades in an area of high contact stresses in the dovetail. Additional cracked blades were found using nondestructive inspections developed after the first accident. Although the blades had been shot peened, many of the blades had relaxed compressive residual stress profiles at the surface, making them more susceptible to fatigue crack initiation under the combined effects of loading/friction changes over time, coating condition, surface condition, and engine operational differences. Flight cycle estimates based on striation counting on the fracture surfaces revealed that blades with normal residual stress profiles had been overhauled after cracks had initiated, masking the original surface condition. As a result of investigation findings, new procedures were developed, including more frequent dovetail lubrications, improved visual inspection procedures, and new ultrasonic testing and eddy current procedures, which were implemented to reduce contact stresses in the dovetail and to detect any potential cracks that might develop in the dovetail before blade fracture.

Keywords Low-cycle fatigue · LCF · Titanium alloy · Residual stress · Fan blade · Turbofan engine

Introduction

On April 17, 2018, Southwest Airlines flight 1380, a Boeing 737-7H4 airplane powered by two CFM International (CFMI) CFM56-7B24 turbofan engines, experienced a left engine fan blade fracture and loss of engine inlet and cowling during climb at about flight level 320.¹ Fragments from the engine inlet and cowling² struck the wing, fuselage, and one cabin window, resulting in a depressurization. The flight crew conducted an emergency descent and landed at Philadelphia International Airport, Philadelphia, PA. Of the 144 passengers and five crewmembers onboard, one passenger received fatal injuries and eight passengers received minor injuries. The airplane sustained substantial damage.

A similar fan blade fracture had occurred nearly two years earlier. On August 27, 2016, another Boeing 737-7H4 airplane powered by two CFMI CFM56-7B24 turbofan engines, operating as Southwest Airlines flight number 3472, had experienced a cabin depressurization after a left engine fan blade fracture and loss of engine inlet while climbing through flight level 310. The flight crew declared an emergency and diverted to Pensacola International

M. R. Fox (✉)
National Transportation Safety Board, Washington, DC, USA
e-mail: FOXM@ntsb.gov

W. R. Rossey Jr.
General Electric, Evendale, OH, USA

M. Raguet
Safran Aircraft Engines, Moissy-Cramayel, France

¹ Flight level is a measure of altitude at 100-foot increments above mean sea level based on differential pressure measurements in accordance with a standard atmospheric pressure model.

² The inlet and cowling are aerodynamic components of the airplane structure associated with the engine but designed by the airframe manufacturer. The inlet is in front of the engine and serves to guide air into the engine, and the cowling is comprised of panels that surround the engine aft of the inlet.

Airport (PNS), Pensacola, Florida. Although the airplane was substantially damaged, none of the 99 passengers, 1 lap child, and 5 crewmembers onboard reported injuries.

This article will focus on laboratory examinations of the fan blades that were conducted to understand the fracture mechanism and strategies implemented by the engine manufacturer to prevent future fan blade fatigue fractures. Additional details of the laboratory examinations are presented in Materials Laboratory Factual Report 17-043 and Materials Laboratory Factual Report 18-049 available in the public docket associated with the respective accident investigation [1, 2]. For additional information about the overall accident investigation and safety recommendations to the Federal Aviation Administration, Southwest Airlines, and the European Aviation Safety Agency, see Aviation Accident Report NTSB/AAR-19/03 published by the National Transportation Safety Board (NTSB) [3].

About the Engine

Twenty-four titanium alloy Ti-6Al-4V fan blades are located at the front of the CFMI CFM56-7B24 engine (Fig. 1). The fan blades are held in slots in the Ti-6Al-4V fan disk, and Alloy 718 shims are positioned between the contact faces of the fan blade and fan disk. An elastomer-coated Ti-6Al-4V spacer is also inserted in each fan disk slot to provide radial constraint. Aluminum alloy platforms with elastomer seals are assembled between the fan blades to guide airflow into the engine and provide circumferential restraint. The portion of the fan blade extending radially outward from the platform is the airfoil, and the remainder

of the blade is the root. The root end of the fan blade has a flattened teardrop-shaped cross section, known as the dovetail, which is the portion of the blade root that is held within the fan disk slot (Fig. 2).

During blade manufacturing and any subsequent blade overhaul, the surfaces of the fan blade airfoil and root are shot peened. The shot-peening process improves blade service life by introducing a local compressive stress at the surface that helps prevent fatigue crack initiation from the surface [4]. After shot peening, the dovetail contact faces are grit-blasted to prepare the surfaces for application of a Cu-Ni-In coating, which is subsequently applied using a plasma spray process. Finally, a coating of MoS₂ dry-film lubricant is applied to the Cu-Ni-In dovetail coating. A coating of MoS₂ dry-film lubricant is also applied to the contact surfaces of the as-manufactured shims where they contact the fan disk slot.

Relubrication of fan blade dovetails and shims has been added at periodic intervals as part of the maintenance program for the engine. During the relubrication process, inspections for cracks are completed, and indications of cracks are cause for removal from service. Additionally, damage such as airfoil impact damage or dovetail coating damage that exceeds specified limits causes the blade to be removed from service and sent for overhaul. The overhaul process includes stripping the Cu-Ni-In dovetail coating, inspecting the blades for cracks and other damage, repairing airfoil damage as needed, shot-peening the airfoil and root, grit blasting the dovetail contact surfaces, and reapplying the dovetail coating and dry-film lubricant. Brush-on or spray-on dry-film lubricant is also applied to

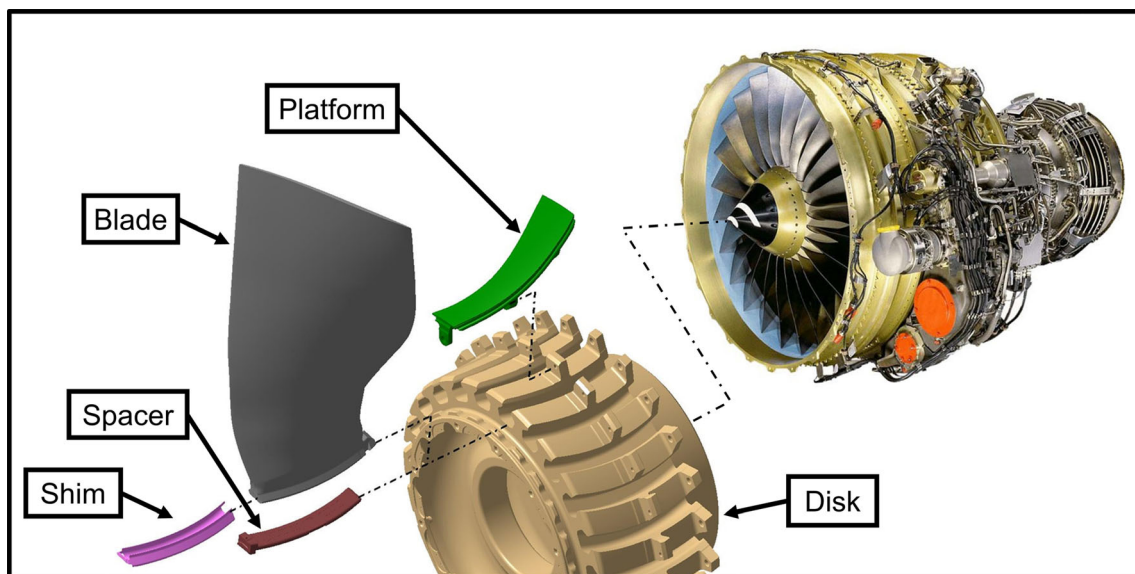
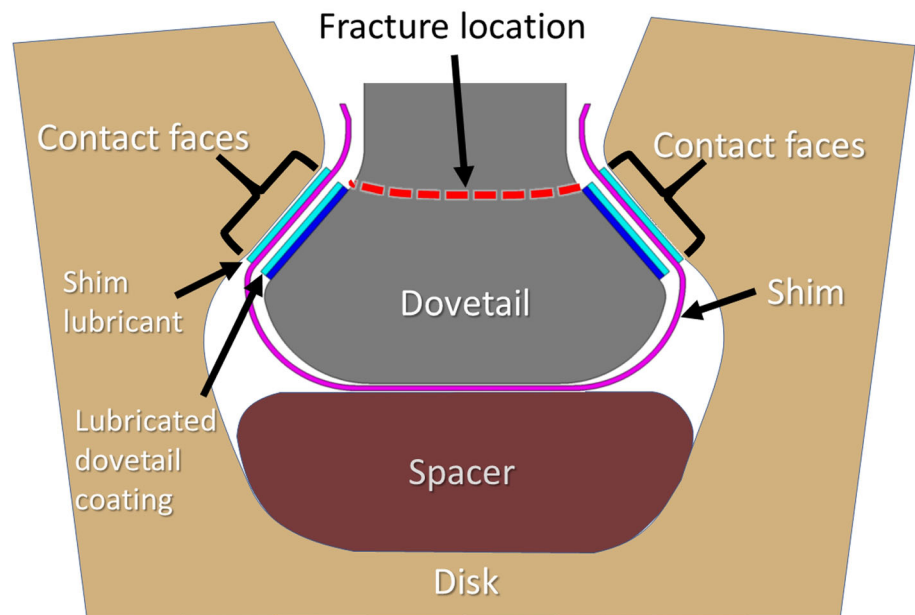


Fig. 1 CFMI CFM56-7B engine with expanded view of fan assembly components adapted from a CFMI exhibit presented at the NTSB investigative hearing

Fig. 2 Fan blade dovetail cross section diagram as presented at the NTSB public meeting convened to discuss and adopt NTSB Accident Report NTSB/AAR-19/03



the dovetail and shim contact surfaces each time the fan blades are installed in the fan disk.

As of August 22, 2018, CFM estimated 356,000 fan blades had been delivered for 14,659 CFM56-7B engines operated for around 360 million flight hours. The August 2016 accident was the first time a fan blade had fractured at the root in one of these engines.

Engine Service Histories

All 24 fan blades from the 2016 accident engine had experienced nearly the same service history operating as a complete set with no blades within the set requiring replacement from the time of first installation on another engine in March 1998. In June 2001, the blades were reworked in accordance with CFM International CFM56-7B Service Bulletin 72-0253, which included machining of the dovetail profiles to prevent spalling and wear damage of the dovetail coating at the forward and aft ends of the contact faces. Because of the rework, the part numbers of the blades changed from 340-001-022 to 340-001-027. At the time of the rework, the blades had 11,720 h TSN and 7754 CSN. The reworked blades were installed on the accident engine in July 2001. The total service time for the blades at the time of the 2016 accident was 62,851 h time since new (TSN) and 38,152 cycles since new (CSN).

Similarly, the 24 fan blades from the 2018 accident engine also had experienced the same service history operating as a complete set with no blades within the set requiring replacement from the time of first installation on another engine in March 2001. The blades were manufactured as part 340-001-026-0 blades and were later

changed to part number 340-001-038-0. The part number 340-001-026-0 blades, introduced in CFM International CFM56-7B Service Bulletin 72-0253, were manufactured with the dovetail profiles that had been redesigned to prevent the dovetail coating spalling and wear damage that had been observed in the part number 340-001-022 blades. At the time of the 2018 accident, the blades had accumulated 55,471 h TSN and 32,636 CSN.

The original fan assembly design for the CFM56-7B engine did not include fan blade shims in the assembly. The engine manufacturer later incorporated shims into the assembly for fan disks manufactured after 2004. Blade sets from both engines had operated without shims early in their life and were installed in assemblies with shims in 2007 and 2012 for the 2016 and 2018 accident blade sets, respectively.

The fan blades from the 2016 accident were last overhauled in June 2007 and had accumulated 17,956 flight cycles since overhaul. Engine records showed the fan blades had received periodic lubrication since 2001, representing most of their time in service. The Aircraft Maintenance Manual stated at the time of the accidents that the blades and shims should be lubricated at intervals not to exceed 5000 hours or 3,000 cycles, whichever occurs first. A review of maintenance records showed the blades had been relubricated in accordance with maintenance manual instructions. Early in the blade life, however, relubrication of the fan blades was not a required maintenance item. The first relubrication for the accident blades occurred in May 2001 after the blades had accumulated 11,242 hours TSN and 7452 CSN.

The fan blades from the 2018 accident were last overhauled in September 2012 and had accumulated 10,712

flight cycles since the blade overhaul. The blades had been overhauled one time prior in April 2004 and had accumulated 26,511 flight cycles since the 2004 overhaul. Engine records reviewed since 2004 showed the fan blades from the 2018 accident also had been relubricated in accordance with maintenance manual instructions.

Procedure

After each engine failure event, the accident airplane was initially examined by an NTSB-led team at the respective airport where each airplane had landed. The blades were numbered sequentially counterclockwise (as viewed looking aft) starting with a reference position on the fan disk. After the initial examinations, the fan blades and fan blade shims, spacers, and platforms were disassembled from the failed engine and together with recovered fan blade fragments were shipped to the NTSB Materials Laboratory in Washington, DC, for further investigation.

Upon receipt at the NTSB Materials Laboratory, the submitted components were photographed to document the as-received condition. Next, the components were examined visually and under optical magnification using a Nikon SMZ1500 optical stereomicroscope. Magnified optical images of the fracture surfaces and other areas of interest identified during the examination were captured using a Keyence VHX-5000 digital microscope. The fracture surfaces on the dovetail side of the fractured blades were further examined using a Zeiss Auriga CrossBeam field-emission scanning electron microscope (SEM). Initial examinations were completed on the dovetail pieces as-received. Examinations continued after the fracture surfaces had been cleaned using acetate tape application and removal followed by ultrasonic cleaning while submerged in acetone. Metallographic specimens were examined using a Zeiss Axio Observer Z1m optical metallograph.

Fracture features consistent with fatigue were identified during the initial stages of the investigations, so the potential for similar cracks in the other examined blades was also considered. In the 2016 accident event, one blade with an intact blade root was sectioned to complete an expedient metallographic examination for cracks in the area identified as the origin area on the fractured blade before nondestructive inspections were initiated. The remaining blades with intact dovetails were inspected using multiple nondestructive techniques including ultrasonic testing (UT), fluorescent-dye penetrant inspection (FPI), and eddy-current inspection (ECI). Because cracks could occur under the dovetail coating, UT was completed primarily from the root end face to detect cracks that might be covered by the dovetail coating. Removal of the dovetail coating would be required to complete FPI and ECI on the

blades and to repeat the UT tests on dovetails after the coating had been removed. However, before stripping the coating, the root end of many of blades was scanned using a Nikon LC15DX laser scanner fitted to a Wenzel LH87 coordinate measurement machine. Selected blades were then rescanned after the dovetail coating was removed, and a differential analysis was used to determine the coating thickness along the length of the dovetail. In the process, the dovetail coating was stripped by soaking the dovetails in concentrated nitric acid until the coating was dissolved.

The blade dovetail surfaces in cracking were etched as needed with a solution of water with 15% concentrated hydrochloric acid and 15% concentrated hydrofluoric acid to facilitate FPI of the blade surfaces for cracks and SEM examinations for microcracks. Surface roughness of the grit-blast area of the dovetail was also measured on one of the blades using a Mahr MarSurf LD 130 surface analyzer and compared to other blades with no cracks.

After the NDI work was completed, transverse sections through the dovetail were prepared in selected blades both with and without crack indications to inspect for cracks and any other anomalies on the unetched surface and to examine the blade microstructure after etching with Kroll's reagent. The microstructures of two blades were further examined using electron backscatter diffraction (EBSD) to map orientations of alpha (HCP crystal structure) grains in the selected blades. The GE Global Research Center in Niskayuna, New York, completed the EBSD grain orientation maps on repolished metallographic samples from a cracked blade and another blade from the same engine with no detected cracks. Each blade with a crack indication was sectioned to open the cracks for fractographic examination, which occurred in laboratories at the NTSB, GE Aviation, and Safran Aircraft Engines.

The condition of the compressive residual stress from the shot peening process was examined by measuring residual stress profiles on selected blades from the accident engines, two exemplar blades removed from different engines, and other cracked blades found during subsequent inspections of the fleet. The X-ray diffraction residual stress measurements were conducted at Lambda Technologies in Cincinnati, Ohio, and at the Safran Materials and Processes Laboratory in Evry Corbeil and Vernon, France, using a two-angle sine-squared-psi technique [5]. The residual stress values obtained at Lambda Technologies were measured parallel to the radial direction, while measurements at the Safran Materials and Processes Laboratory were measured parallel to the longitudinal axis. On one blade, the Safran Materials and Processes Laboratory completed measurements parallel to both the radial and longitudinal directions and obtained similar results. Multiple test locations were selected on each blade, and at each location material was removed electrolytically during the

tests to provide measurements at the surface and at varying depths up to approximately 200 μm (0.008 in).

Findings

In this section, the findings associated with the 2016 accident will be presented in detail followed by a brief description of findings from the 2018 accident focusing on relevant similarities and differences. Finally, a summary of findings associated with cracked blades detected by NDI completed during field inspections or blade overhauls will be described.

In the 2016 accident, blade 23 had fractured in the dovetail at the location indicated in Fig. 2, and most of the remainder of the blade was not recovered. The remaining blades were intact but had impact damage at the leading and trailing edges such as the blades adjacent to blade 23. Many of the shims and dovetails were damaged consistent with blade movement after blade 23 fractured.

The fracture surface on the dovetail piece from blade 23 had indications of a progressive crack that existed before fracture (Fig. 3). A portion of the fracture surface

intersected the dovetail surface at a 90-degree angle and had a curving boundary, features consistent with a progressive fracture mechanism in ductile materials. Unlabeled arrows in the upper image in Fig. 3 indicate the extent of progressive crack growth, which measured up to 2.28 in (57.8 mm) axially and 0.695 in (17.7 mm) deep. The remainder of the fracture surface had matte gray fracture features with prominent shear lips along the edges, features consistent with ductile overstress fracture.

Within the progressive crack growth region, four crack arrest lines were identified in the region bounded by the dashed line in Fig. 3. Ratchet marks were also observed, indicating the crack had initiated from multiple origins along the convex side of the dovetail near the dovetail leading edge. The crack arrest lines were numbered sequentially starting with the line closest to the origin (Fig. 4). The region measured 1.14 in (29.0 mm) long axially at the dovetail surface and extended up to 0.217 in (5.51 mm) deep as measured projected on a plane parallel to the root end face.

Next, the fracture surface was further examined using an SEM, and the fracture mechanism up to the fourth crack arrest line was confirmed to be fatigue. Much of the area

Fig. 3 Dovetail for fan blade 23 showing the fracture surface. Unlabeled arrows indicate the extent of progressive crack propagation, and a dashed line indicates the location of the last crack arrest line associated with well-defined fatigue crack striations. A bracket indicates the fatigue origin area at the convex side of the dovetail. (Ruler in inches.)

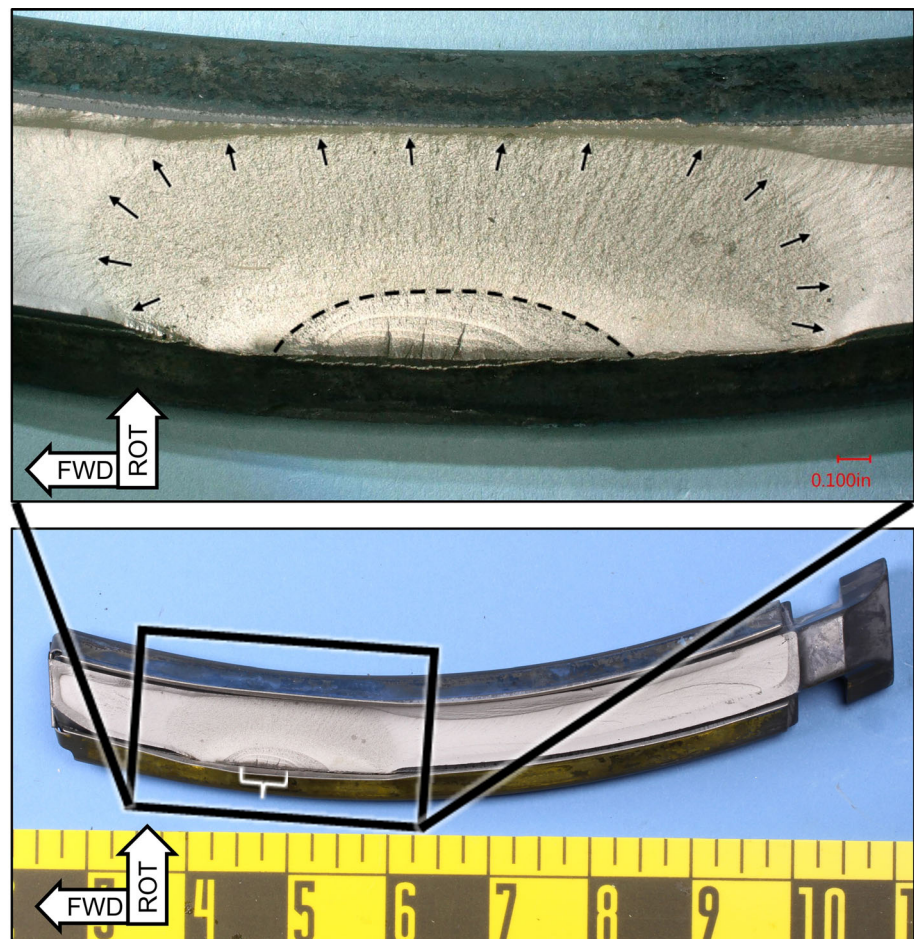
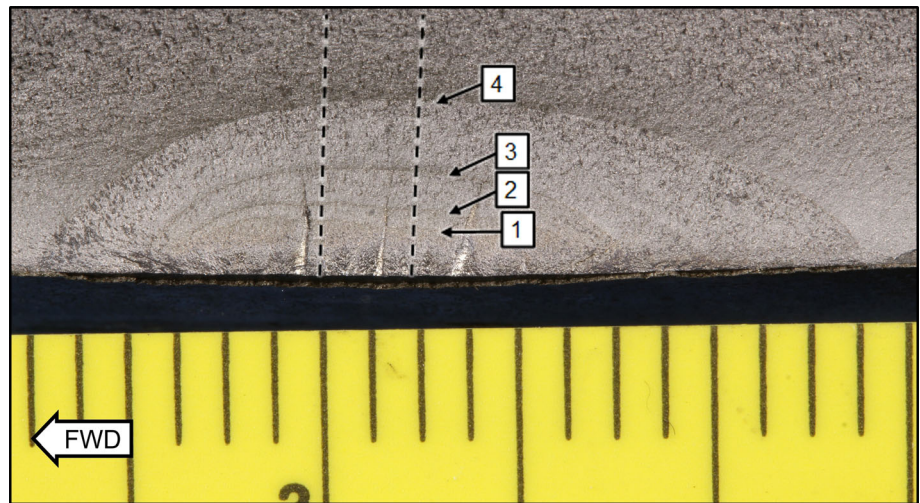


Fig. 4 Fatigue origin area on blade 23. Numbered call-outs indicate locations of crack arrest lines, and dashed lines indicate paths where fatigue striation densities were measured. (Ruler has 1/16-inch increments.)



near the origin was damaged due to relative motion between the fracture faces, but isolated areas of original fracture surfaces with fatigue striations were observed (Fig. 5). Further from the origin area, the fracture features exhibited less damage, and more fatigue striations were observed (Fig. 6). Isolated areas of quasi-cleavage fracture were interspersed within the fatigue striations at crack depths greater than approximately 2.5 mm (0.10 in). At greater crack depths, the fracture features gradually transitioned to more quasi-cleavage features with isolated areas of striations. No discernable striations were observed beyond a crack depth of 8.2 mm (0.32 in). At the progressive crack growth region boundary, the fracture morphology abruptly changed to dimple features consistent with microvoid coalescence associated with ductile over-stress fracture across the remainder of the fracture surface.

The area around the origin was examined closely using imaging with both in-lens and in-chamber secondary-electron detectors and a below-lens backscattered electron detector in composition mode. Fine features near the origin were mostly obliterated by relative movement between the mating surfaces. However, no evidence of any anomalies in the material composition or the adjacent dovetail surface condition was observed during the examination.

In the next stage of the SEM examination, the fatigue striation linear density was measured at locations across the fracture surface along two separate paths (Fig. 4). At each location, the distance in the fracture plane from the dovetail surface was recorded, and an image was taken at a resolution sufficient to resolve approximately 10 to 20 sequential striations within the image frame. The striation linear density, ρ , in terms of number intersected per unit length in the direction of crack growth for that image was then determined using the following equation,

$$\rho = f \frac{(n - 1)}{l} \tag{Eq 1}$$

where n is the total number of sequential striations counted in the image, l is the length from the first to last striation as measured on the image, and f is the magnification factor determined by dividing the measured length of the scale bar on the image by the scale bar reference length. Results of the measurements and recorded distance from the surface were then plotted in a chart showing a general trend of decreasing striation linear density with increasing distance from the fatigue origin, consistent with low-cycle fatigue (LCF) in engine components (Fig. 7). The distances from the origin for crack arrest lines 1 through 4 are also indicated in the striation linear density chart.

Next, a power-law curve with the following form was fit to the data,

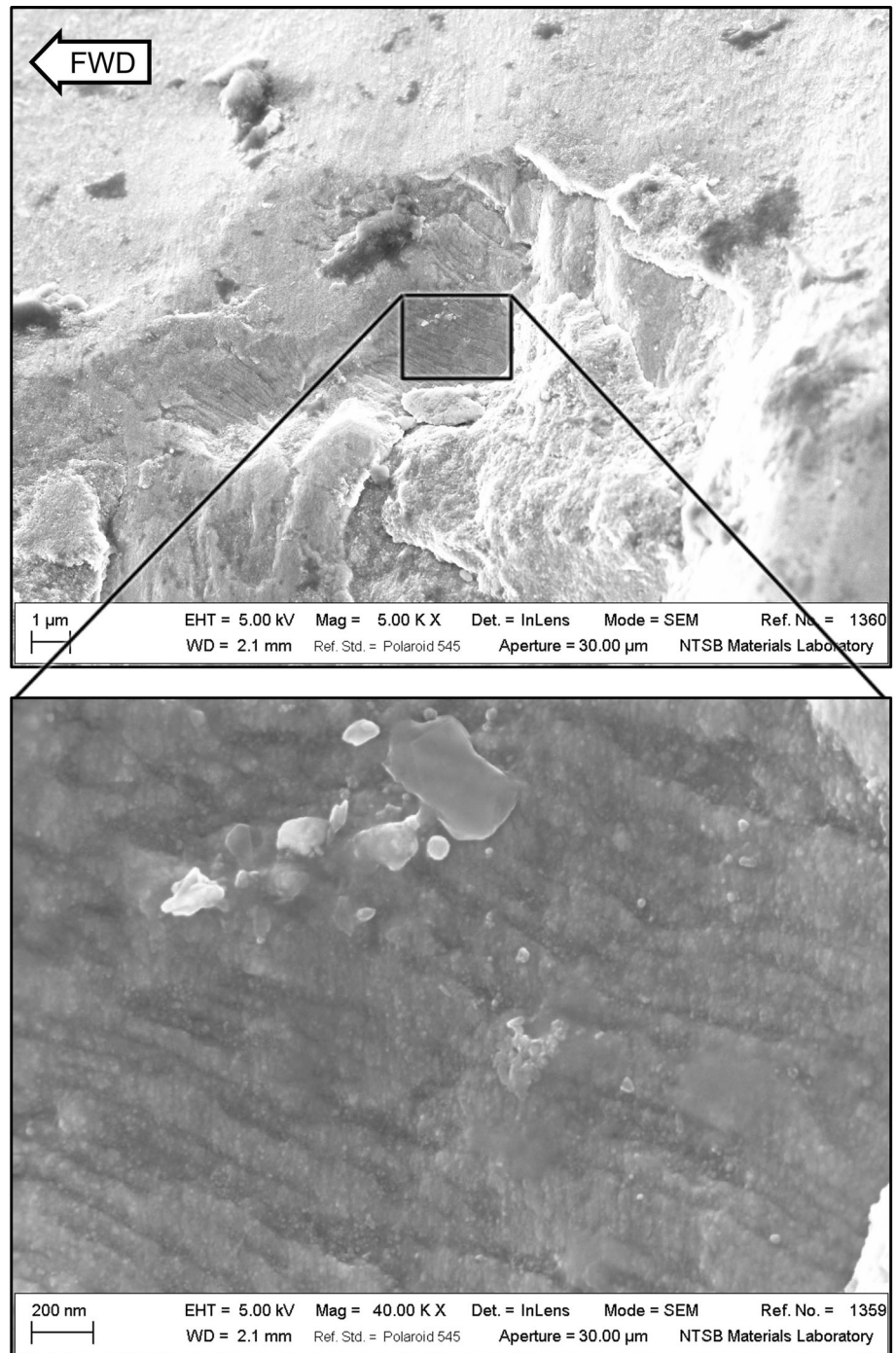
$$\rho = ax^n \tag{Eq 2}$$

where x is the distance from the origin, a is a constant with units of cycles per length to the power of $(1 + n)$, and n is a dimensionless constant. Using Microsoft Excel to determine the curve fit (US customary units were used for the curve fit), the constants a and n were determined to be 9029.9 and -0.656 , respectively. With constants determined for Eq 2, the following integral was used to estimate the total number of striations, N , associated with crack growth from a reference depth of 0.0005 in. (12.7 μm) to the depth of crack arrest line 4 at 0.228 in. (5.79 mm) as measured in the plane of fracture,

$$N = \int_{0.0005}^{0.228} 9029.9x^{-0.656} dx \tag{Eq 3}$$

By solving Eq 3, the total striations associated with crack growth from 12.7 μm (0.0005 in) deep to crack arrest

Fig. 5 Typical fatigue striations observed at 208 micrometers from the convex dovetail surface

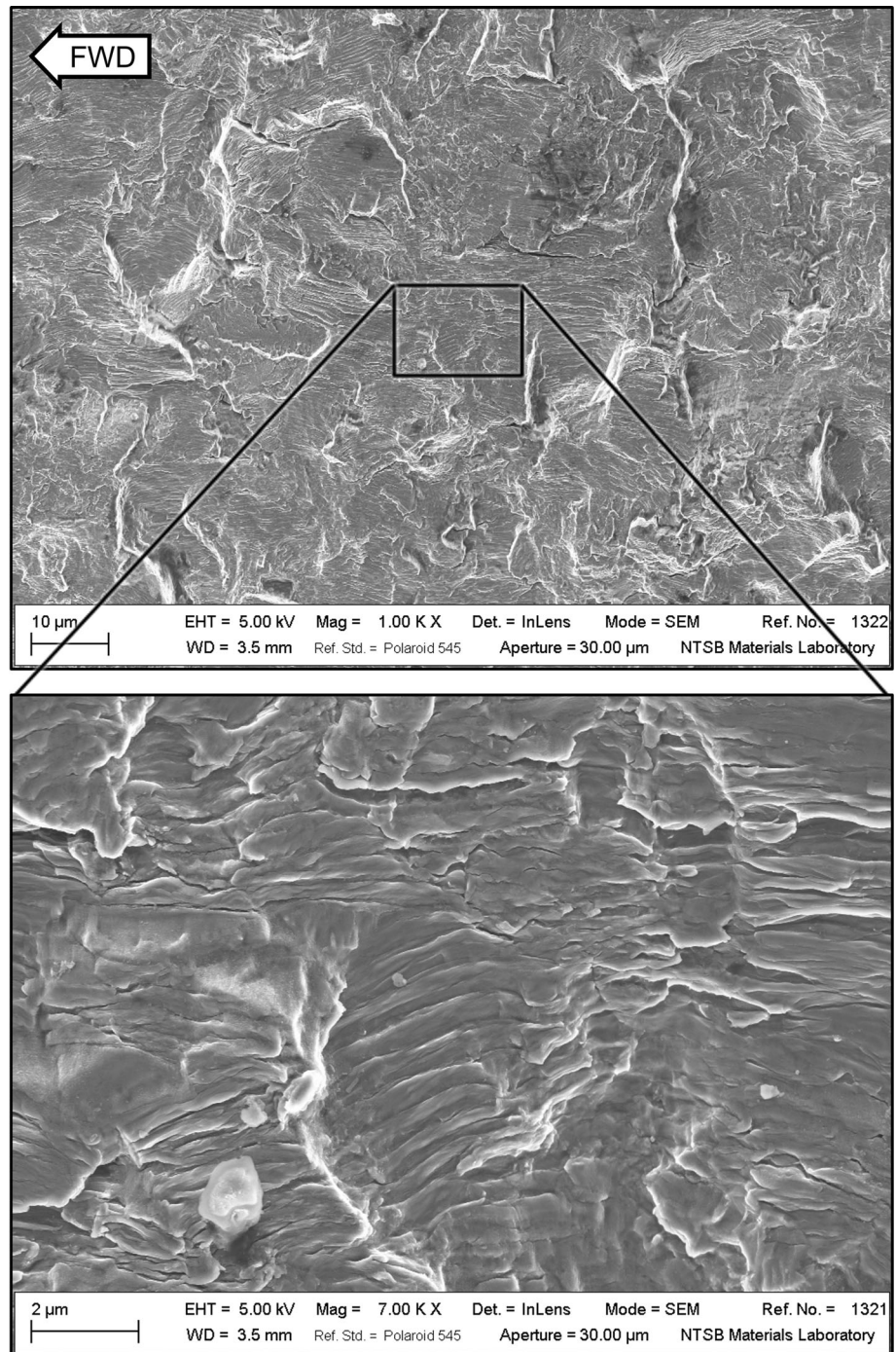


line 4 were estimated to be approximately 14,000. Although striation linear density could not be reliably estimated for the remainder of the progressive crack growth on blade 23 due to the extent of quasi-cleavage features, subsequent analysis discussed below indicated the remainder of the progressive growth beyond crack arrest line 4 occurred during approximately 1,000 flight cycles since the last fan blade relubrication. Since one striation generally represents one engine flight cycle for LCF crack growth in these fan blades, the total number of engine flight

cycles associated with crack growth from a depth of $12.7\ \mu\text{m}$ (0.0005 in) to final fracture was estimated to be 15,000 cycles.

The significance of the crack arrest lines was also explored. Crack arrest lines generally represent a change in stress state, environment, or time interval associated with fatigue crack growth [6]. Blade removal, cleaning, lubrication, and re-installing can affect local stresses after reseating at operational speeds. Therefore, the change in stress state associated with blade relubrication was

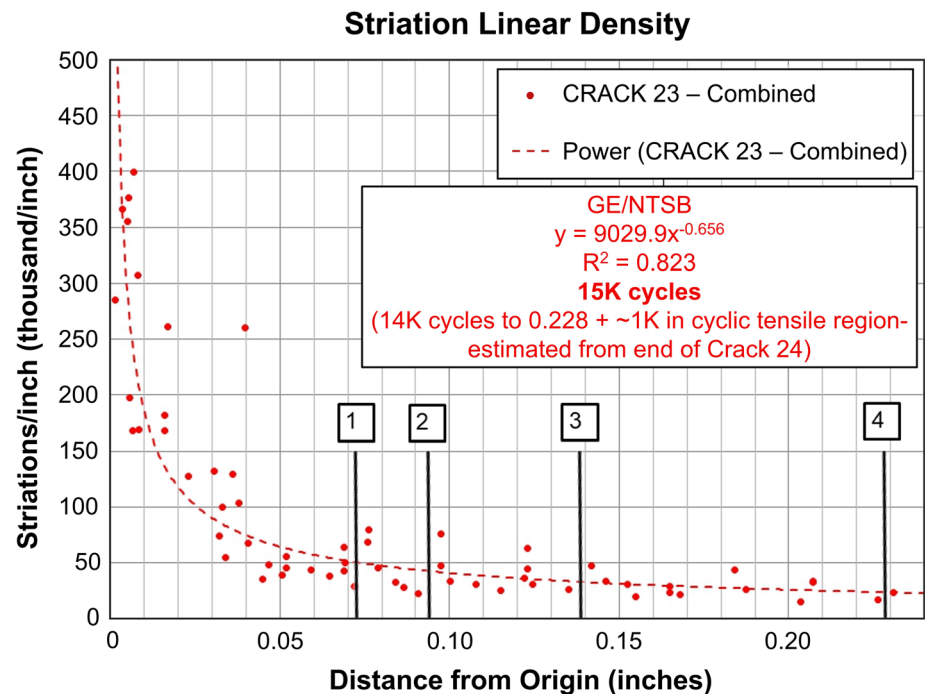
Fig. 6 Typical fatigue striations observed at 2.49 millimeters from the origin.



suspected as the source for crack arrest line formation in this case. By adjusting the limits of integration in Eq 3 to reflect the depths of adjacent crack arrest lines, the number of cycles between crack arrest lines was estimated. The results showed good correlation with the reported relubrication intervals documented in the maintenance records, confirming that the crack arrest lines were likely associated with blade relubrication events. Additionally, a detailed

SEM examination of the fracture surface at the crack arrest lines generally revealed a sudden increase in the striation linear density associated with growth after the crack arrest line compared to the linear density leading up to the crack arrest line. This was consistent with slower crack growth due to a reduced peak stress intensity after blade relubrication, providing further confidence in the interpretation of

Fig. 7 Striation linear density data collected from the SEM examination of the blade 23 fracture surface. Locations of crack arrest lines are indicated, and the equation for the curve fit to the data is shown.



fatigue features and their relation to flight cycles and relubrication intervals.

A visual examination of the fan blades showed eight of the blades including blade 23 had areas of missing dovetail coating on the convex side of the blade near the forward end of the dovetail. On blade 23, the dovetail coating was disbonded and missing at both the outboard and inboard edges of the coating. Gray dry-film lubricant was observed on the surface at the inboard disbond area with linear streaks consistent with brush strokes from the brush-on lubricant application process completed at blade installation, indicating that the area had been disbonded before at least the last installation. Furthermore, the mating interior surface of the blade 23 shim had a contact pattern that mirrored the damaged dovetail coating shape. Areas that mated to the disbonded coating areas were not worn, indicating that the shim had not been in contact with a coating at any time since its installation at one of the last two blade relubrications.

The next steps in the examination focused on blade 24 since it had dovetail coating damage like blade 23 and was from the same forging lot. No evidence of cracks was detected using an optical stereomicroscope but given the location of the crack in blade 23, it was considered possible that cracks could be hidden under the dovetail coating. Therefore, a transverse cut was made through the dovetail in potential cracking to prepare a metallurgical sample of the dovetail cross section. The cross section was examined on a metallograph in both the unetched condition and after etching with Kroll's reagent. The examination revealed

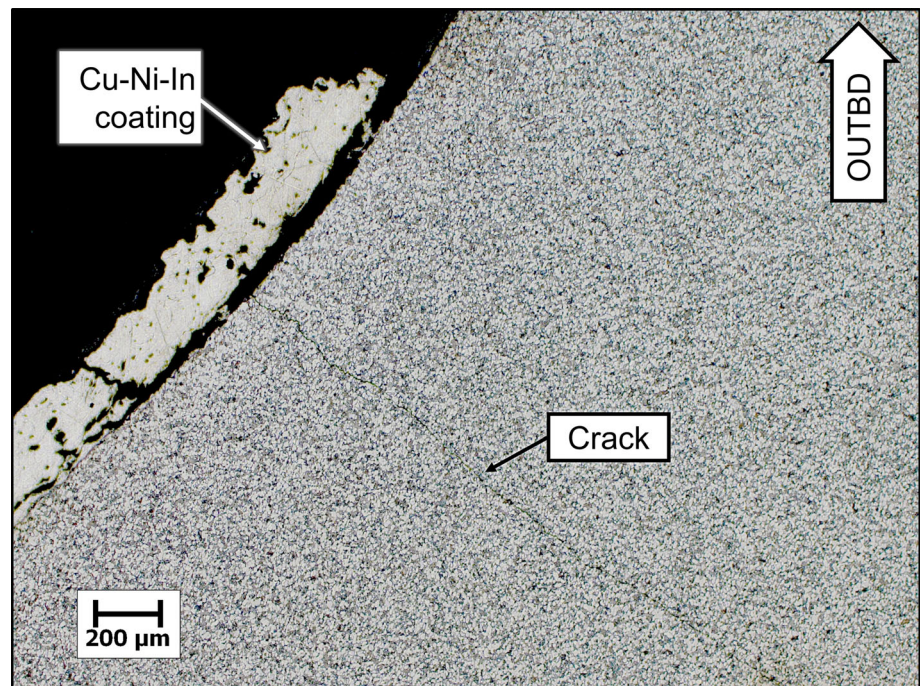
cracks emanating from the grit-blasted surface of the dovetail in an area that was covered by the intact dovetail coating (Fig. 8). The etched microstructure appeared uniform with an even mix of alpha and alpha plus beta grains as expected for the specified material. No surface anomalies such as distorted grains or alpha case were observed on the surfaces.

A battery of nondestructive tests was conducted on the remaining fan blades to determine if additional blades were cracked. Several UT methods were applied to detect cracks with the coating intact on most of the blades. The UT tests were repeated after the coating was removed, and it was found that the dovetail coating could introduce noise into the signal response. However, the UT tests with the coating intact indicated the presence of cracks in 2 of the blades.

After the dovetail coatings were chemically stripped from blades 1 through 22, FPI and/or ECI were completed on the blades. The ECI method proved to be the most sensitive technique, detecting cracks in an additional 4 blades.

Next, the dovetail surfaces were examined on selected blades using an SEM. The selected blades included 5 blades with NDI crack indications and 6 blades with no indications from FPI or ECI. In the 6 blades with no crack indications, a network of parallel microcracks was observed on the surface (Fig. 9). The microcracks were in a band near the boundary of the grit-blast region that had been covered by the dovetail coating. In the blades with crack indications, adjacent microcracks appeared to link together to form a crack-like feature associated with the

Fig. 8 Micrograph of the blade 24 cross section through the dovetail showing a crack emanating from the convex dovetail surface under the dovetail coating. Etched with Kroll's reagent



NDI response. All cracks and microcracks were in the grit-blast surface of the dovetail contact face, and no cracks or microcracks were observed in the adjacent shot-peened areas.

Each detected crack was opened by lab fracture, revealing features consistent with high-alternating stress, LCF emanating from multiple origins. Crack depths for detected cracks ranged from 0.229 mm (0.00901 in) in blade 1 to 3.20 mm (0.126 in) in blade 24. Fatigue striation estimates were completed on each of the cracks using the method described above with the appropriate power-law constants and integration limits for each case, and the estimated number of flight cycles associated with growth of each crack ranged from 4000 cycles in the smallest cracks to 16,000 cycles for the crack in blade 24. These results indicated the crack in blade 24 initiated before the crack in blade 23 but was growing at a slower rate. The difference in crack growth rate was likely related to differences in the crack aspect ratios (crack depth divided by half the length at the dovetail surface). The aspect ratio for the blade 23 crack fatigue region was 0.381, while the aspect ratio for the blade 24 fatigue crack was 0.563.

To determine the condition of the compressive residual stress imparted by the shot peening process, nine blades, including the fractured blade, blades with cracks, and blades without cracks, were selected for testing to determine the residual stress depth profile for comparison to the expected profile for a shot-peened blade. Most of the tests were conducted on the grit-blasted contact face of the dovetail near the area of cracking, but other areas of the

dovetail contact face and adjacent shot-peened root areas were tested on multiple locations on the convex and concave sides of a cracked blade and a blade without cracks. Results for approximately 80% of the test locations showed residual stress profiles where the peak compressive stress was less compressive than the expected peak at -500 MPa, including all tests of cracked blades near the area of cracking (Fig. 10). In the adjacent shot-peened areas of the blade root, residual stress profiles comparable to the reference profile were obtained.

Although aligned alpha grains are not usually associated with crack initiation in titanium alloys with significant beta phase content such as the Ti-6Al-4V alloy in this case, the alpha grain orientation was mapped in cracking on a transverse cross section of cracked blade 24 and a similar area on a blade with no cracks. Results showed a relatively random and even distribution of alpha grain orientations in the areas mapped. No groups of grains with similar orientations (colonies of aligned alpha grains) were observed.

During the examination, dovetail coating thickness had been determined on many of the blades by comparing data from 3D laser scans of the blade roots before and after the coating was stripped. Results were then mapped showing the differential between the data points from the two scans. The maps showed variations in the coating thickness along the length of the blade dovetails, and many of the blades had coating thickness values in some areas that exceeded the maximum new-make value specified in the manufacturer's coating instructions. (This may not be directly

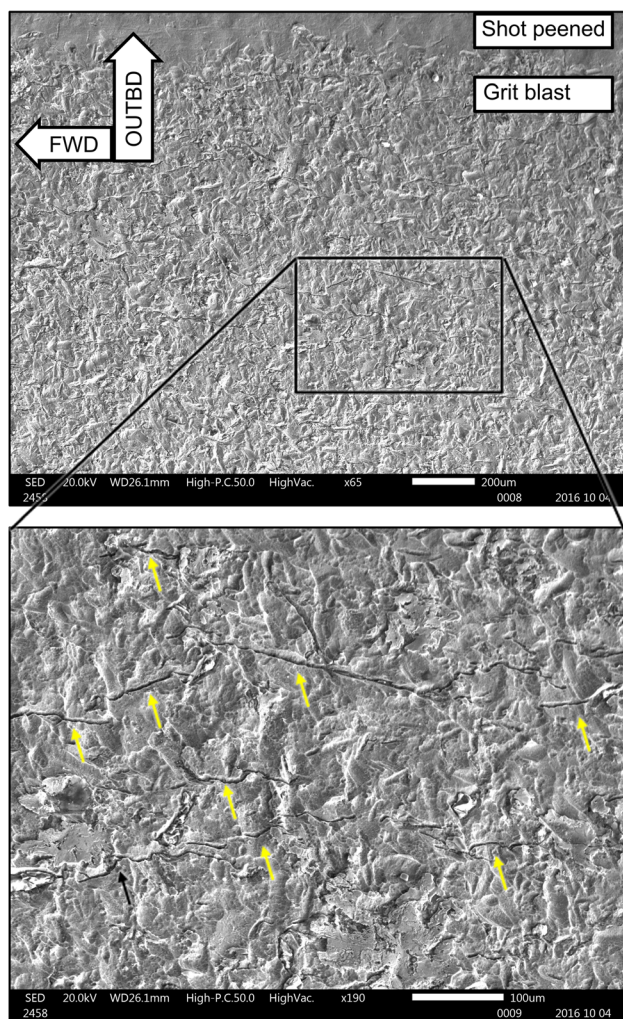


Fig. 9 Network of parallel microcracks (indicated by yellow arrows) observed on the grit-blasted surface of a blade with an intact dovetail after the dovetail coating was removed. No cracks were detected by NDI

comparable to new-make data as changes can occur in the field.)

To help with a preliminary assessment of the population at highest risk of cracking, a fan blade with the same part number and forging lot as blade 23 and another high-time blade that had been manufactured after the dovetail modification had been implemented were obtained from the fleet for examination. After a combination of NDI and SEM examination of the dovetail surfaces was completed, no cracks or microcracks were detected in either of these exemplar blades. Residual stress profiles were also measured on each exemplar blade, and both profiles had compressive stress profiles that were comparable to the reference profile.

The fan blade that fractured in the 2018 accident had fractured features that were very similar to the 2016 accident. The fracture occurred in the dovetail of blade 13, and

multiple origins were located at the convex contact face but further forward near the leading edge (Fig. 11). SEM examination of the fracture surface confirmed the fracture features were consistent with LCF. Six crack arrest lines were identified on the fracture surface, and striation count estimates between crack arrest lines corresponded closely with the flight cycles associated with the relubrication intervals. The total number of flight cycles associated with crack growth from 12.7 μm (0.0005 in) to fracture was approximately 20,000 cycles.

Maintenance records showed the blades had been overhauled 10,712 cycles before the accident, which means the blades had been overhauled after the crack had initiated in blade 13. The crack was not detected during the overhaul FPI. (ECI was not developed nor required for this location at the time.) The coating damage near the leading edge that had been observed in many of the blades from the 2016 accident was not observed in the 2018 accident blades, and the residual stress profile for blade 13 was comparable to the reference residual stress profile. However, since the blades were shot peened and recoated during the overhaul process, the coating condition and residual stress state at the time of blade fracture were not considered representative of the conditions at the time of crack initiation.

After the 2016 accident, additional inspections as described in the next section were developed and implemented to detect cracks in other fan blades in the fleet. As of August 2019, 3 cracked blades were found during blade relubrication, and 12 cracked blades were found during blade overhaul; detecting cracks that were significantly smaller than the cracks found in the liberated blades. The cracked blade population includes blades that were installed on aircraft operated by multiple foreign and domestic operators. Most of the cracked blades were originally manufactured with the early dovetail design, but some cracked blades had been manufactured later after the dovetail had been changed to prevent spalling and wear damage to the dovetail coating. The cracks were mostly located on the convex side of the dovetail near the leading edge as found in the two accident cases, but one blade had a crack on the concave side near the trailing edge of the contact face, and one blade had cracks on both sides. Most of the blades had accumulated more than 30,000 cycles since new at the time of crack detection, but one of the cracked blades had accumulated 19,497 cycles since new.

Residual stress profiles were measured on six of the first seven cracked blades found during inspections. Three of the blades had residual stress profiles with a peak compressive stress that was less compressive than the reference profile. The remaining blades with normal profiles and the untested blade had been overhauled in the time since the cracks had initiated.

Fig. 10 Residual stress profiles of fractured and cracked blades measured on the convex side near the area of cracking. The blue line shows a reference profile of a shot-peened surface for comparison

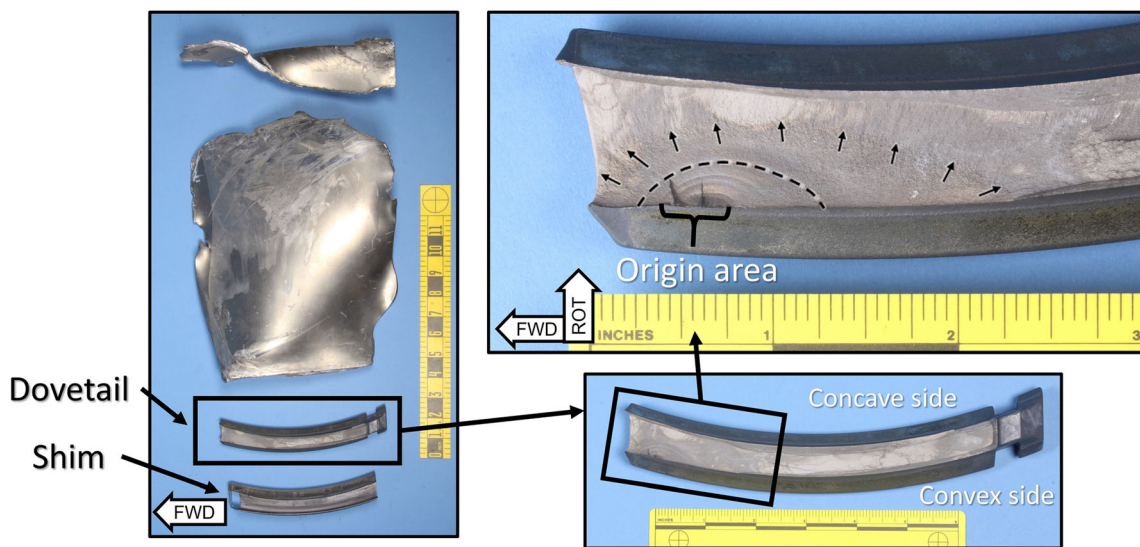
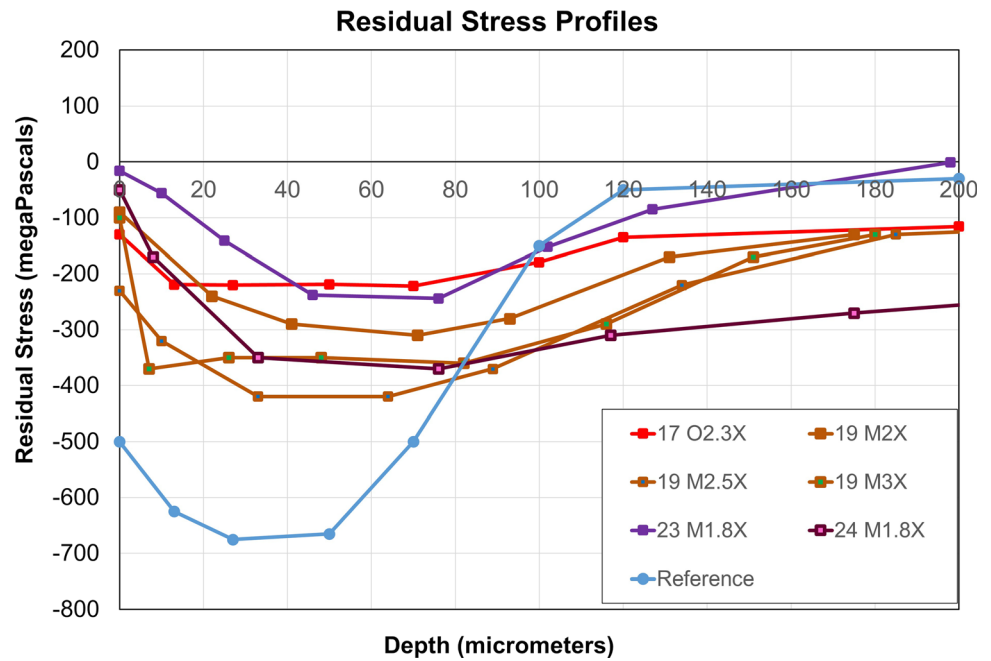


Fig. 11 Overall view of the blade 13 fracture from the 2018 accident (left image) with closer views of the fracture surface on the dovetail (right images). Arrows in the upper right image indicate the extent of

progressive crack propagation, and a dashed line indicates the last of 6 crack arrest lines

Discussion

Examinations of the fractured and cracked blades showed LCF cracks initiated from multiple origins at an area subject to high contact stresses on the dovetail. Additional data gathered during the accident investigations helped improve the understanding of the issues related to the fatigue initiation. Although both accidents occurred on airplanes operated by Southwest Airlines, additional cracked blades were found on engines owned by other airlines, indicating

the issue was not related to any specific operator. Cracks also occurred in blades from multiple forging lots and with multiple part numbers, indicating the issue was not specific to any manufacturing lot. Although dovetail coating damage, thickness variations, and evidence of excess thickness were observed on many blades from the 2016 accident, other cracked blades were found with conforming dovetail coatings.

A key finding in the examinations was the relaxed residual stress condition found on many of the cracked

blades and one fractured blade. Although some cracked blades and one fractured blade did not have a relaxed residual stress condition, those blades had been overhauled in the time since crack initiation, which would have reset the residual stress profile upon peening. The relaxation effectively increased the expected peak stress concentrations on the grit-blast dovetail surface during fan blade operation, thereby contributing to fatigue initiation.

Several possible causes for relaxation of the residual stress imparted by the shot peening process were considered, including excessive removal of surface material, exposure to high heat, or exposure to high tensile stress. However, no evidence of excessive material removal such as a step at the edge of the grit blast surface was found. The dovetail plasma spray coating process was considered as a potential source for high heat exposure, and post-accident testing at CFMI showed that coating deposition without proper cooling could cause residual stress relaxation like that observed on many of the cracked blades. Since the relaxed residual stress profiles were only found on dovetail contact faces that had been shot-peened, grit blast, and coated and since normal profiles were found on adjacent shot-peened-only areas not subject to contact, sources of potential high contact stress were investigated with consideration for investigation findings and fleetwide service history.

The investigative group visited the shop that performed an overhaul before crack initiation on each of the cracked and fractured blades and did not uncover conclusive evidence of excessive heating during dovetail plasma spray coating operations. However, changes in equipment, processes, and personnel had occurred in the years between crack initiation and fracture in the accident blades, which inhibited the ability to conclusively identify and replicate a problem or anomaly in the process that could have contributed to the residual stress relaxation.

Potential sources of elevated operational stress at the dovetail contact face as a cause for the stress relaxation were also considered, including variations in engine operation and coating condition. Early in the life of the CFM56-7B engine model, relubrication of the fan blade dovetails was not required during regular maintenance. Many of the older blades from this engine type were not lubricated until regular lubrication at 5,000 hours or 3000 cycles became part of the maintenance plan in 2000. Regular lubrication helps to decrease the stresses in the dovetail and reduces the coating wear rate. Blades operated for long times before blade relubrication procedures were implemented likely experienced higher peak stresses on the dovetail and increased probability of coating damage. However, some cracked blades found during inspections were lubricated at regular intervals throughout their lifetime. Although potential sources of elevated operational stress were

identified during a post-accident CFMI stress analysis, the findings suggested it is unlikely that operational stresses alone were sufficient to cause the observed relaxation in residual stress.

Ultimately, multiple factors affecting both operational and residual stresses on the dovetail contact face may have contributed to fatigue cracking in the fan blades. The potential for higher operational stresses on the dovetail contact face existed due to higher friction levels when operated without lubrication or a shim, coating spalling, and variations in coating thickness, and the expected fatigue margin was reduced in some blades due to a relaxed compressive residual stress profile. The NTSB found that “the low-cycle fatigue crack in the fan blade dovetail initiated because of higher-than-expected dovetail stresses under normal operating load.”

Conclusion

As a result of the investigation findings, many actions have been implemented to detect dovetail cracks before blade fracture. Procedures and tools were developed to improve visual inspections of the coating condition, incorporate ECI in the blade overhaul process, and conduct UT during each blade relubrication. Additionally, one-time UT inspections were required for high-time blades. Initially, priority was assigned to identifying and inspecting fan blades with the highest number of flight cycles since last overhaul, which were at highest risk based on the early investigation data. As more data were gathered, all fan blades manufactured before the dovetail modification were targeted for inspection, which added priority to inspecting the oldest blades in the fleet with the highest expected accumulated cycles and at highest risk of having experienced high contact stress levels particularly early in their service life. Finally, repetitive UT inspections every 1,600 flight cycles were required for all fan blades in CFM56-7B engines once the blades had accumulated at least 17,000 cycles since new. Since the fan blades are relubricated during the repetitive inspections, relubrication intervals also were reduced for the inspected blades. The NTSB concluded, “the requirement to perform an ECI at the time of fan blade overhaul and an ultrasonic inspection at the time of blade relubrication should enable cracked fan blades in CFM56-7B engines to be detected and removed from service before the cracks reach a critical size and the blades fracture.”

Acknowledgment In accordance with Title 5 Code of Federal Regulations §2635.807(b)(2), the views expressed in this article do not necessarily represent the views of the National Transportation Safety Board or the United States, nor do the views represent those of CFMI (Safran Aircraft Engines and GE Aviation). The authors acknowledge contributions by Pierre Scarfo (NTSB Powerplants

Investigative Group Chairman) and Bill English (NTSB Investigator-in-Charge). Additionally, the authors recognize contributions to the laboratory examination from Mike Lindamood, Valerie Gros, Dave Zigan, Jim Dobbs, Gary Tuss, Mike Germani, Eric Allred, Kyle Gustafson, Vincent Ecalle, Julien Ballester, and Stephane Otin representing Southwest Airlines (airplane operator), Safran Aircraft Engines (engine manufacturer), GE Aviation (engine manufacturer), The Boeing Company (airplane manufacturer), Collins Aerospace (inlet manufacturer), the Federal Aviation Administration (regulator), and the Bureau d'Enquêtes et d'Analyses pour la sécurité de l'aviation civile (French organization for safety investigations). In addition to work completed at the NTSB Materials Laboratory, work during subsequent phases of the examinations took place at the GE Engineering Materials Systems in Evendale, Ohio, and at the Safran Aircraft Engines Failure Analysis Laboratory in Moissy-Cramayel, France.

References

1. M.R. Fox, *Accident Docket DCA16FA217, Materials Laboratory Factual Report 17-043*. (National Transportation Safety Board, Washington, DC, 2018)
2. M.R. Fox, *Accident Docket DCA18MA142, Materials Laboratory Factual Report 18-049*. (National Transportation Safety Board, Washington, DC, 2018)
3. Left Engine Failure and Subsequent Depressurization Southwest Airlines Flight 1380 Boeing 737-7H4, N772SW, Aircraft Accident Report NTSB/AAR-19/03, NTIS PB2019-101439, National Transportation Safety Board, Washington, DC (2019)
4. X. P. Jiang, C. S. Man, M. J. Shepard, and T. Zhai, *Effects of Shot-Peening and Re-Shot-Peening on Four-Point Bend Fatigue Behavior of Ti-6Al-4V*, Mater. Sci. Eng. A, Vol. 468-470, Elsevier (2007) 137-143
5. Residual Stress Measurement by X-Ray Diffraction, 2003 Ed., HS-784/2003, SAE International, Warrendale, Pennsylvania (2003)
6. W. T. Becker, R. J. Shipley, Eds., *Failure Analysis and Prevention*, Vol 11, ASM Handbook, ASM International, Park, OH, 2002, p 633

Publisher's Note Springer Nature remains neutral with regard to jurisdictional claims in published maps and institutional affiliations.

Springer Nature or its licensor (e.g. a society or other partner) holds exclusive rights to this article under a publishing agreement with the author(s) or other rightsholder(s); author self-archiving of the accepted manuscript version of this article is solely governed by the terms of such publishing agreement and applicable law.